Available online at www.sciencedirect.com
SCIENCE DIRECT®
Journal of Power Sources 130 (2004) 213–220
JOURNAL OF POWER SOURCES
www.elsevier.com/locate/jpowsour

Effect of Al-doping on lithium nickel oxides

T. Amriou [a,b,*], A. Sayede [a,b], B. Khelifa [b], C. Mathieu [b], H. Aourag [a,c]

[a] *Computational Materials Science Laboratory, Physics Department, University of Sidi-Bel-Abbes, Sidi-Bel-Abbes 22000, Algeria*
[b] *Faculte Jean Perrin, Université d'artois, SP18 Rue Jean Souvraz, 62307 Lens cedex, France*
[c] *LERMPS, Université de Belfort-Montbeliard, Site des Sevennans, 90010 Belfort, France*

Received 29 January 2003; received in revised form 17 November 2003; accepted 24 November 2003

Abstract

The electronic structures of $LiNiO_2$, $LiAlO_2$ and $LiNi_{0.5}Al_{0.5}O_2$ are investigated using density-functional theory (DFT) in the local-density approximation (LDA). The effect of lithium intercalation and the influence of aluminium doping on the structure and electrochemical properties of $LiNiO_2$ are discussed. An increase in the open circuit voltage is observed with Al doping in $LiNi_{0.5}Al_{0.5}O_2$ compound.

Keywords: Rechargeable batteries; Transition-metal oxides; Average intercalation voltage; Linearized augmented plane wave; First-principle's calculation

1. Introduction

Rechargeable lithium batteries have been intensively studied over the last and the present decades and are now available as competitive energy source [1]. Therefore, further improvements are anticipated concerning the environmental compatibility, energy density, specific energy, cycling behavior, etc. To achieve some of these goals, a great number of experimental works has been devoted to the structure characteristics and the specific properties of intercalation compounds [2–5]. However, there still exist many unanswered questions on the performance of these materials. Indeed, experiments in this area require an immense amount of time and manpower for synthesis, characterization and cycling. In parallel, a significant volume of theoretical studies has been devoted to the calculation of band structure of intercalation compounds using different computational methods [6–10].

Lithium metal oxide with the layer structure $LiMO_2$, (M = 3d transition metal) [11–13] has drawn considerable attention for lithium-ion cell application due to its high energy density and capacity. It has, however, a few disavantages, e.g. stoichiometric $LiNiO_2$ is difficult to synthesize. When used as cathode material, $LiNiO_2$ is less stable structurally upon cycling and shows severe capacity fading, etc. [14,15]. Various attempts have been made to minimize these problems. Recently, lithium metal oxides with a mixture of cations on the metal site ($LiM_{1-y}M'_yO_2$) are currently of much interest as rechargeable battery cathodes as they may offer the possibility to improve properties over those of single-metal oxides ($LiMO_2$) [15–20].

Compared to the transition metals, Al has not received wide attention as a dopant, with only few report on $LiAl_yM_{1-y}O_2$ (M = Co, Ni) system [21–23]. Al substitution of the transition-metal cation has been shown theoretically [6–10] and experimentally [2–5] to increase the cell voltage. This effect has been verified for $LiAl_yCo_{1-y}O_2$ solid solution [24]. Moreover, $LiAlO_2$ is stable in the α-$NaFeO_2$ structure at temperature below ∼600 °C [25] and it has a stabilizing effect of the structure as reported for monoclinic $LiAl_yMn_{1-y}O_2$ [26]. Its low cost and low density makes $LiAlO_2$ attractive as an intercalation compounds constituent.

The important features of a lithium/metal-oxide compound for battery applications include the voltage at which it exchanges lithium, the amount of lithium that can be reversibly intercalated and the stability of the material. The first two properties determine the energy density and the latter limits the lifetime of the battery. Ceder et al. [24,27] have demonstrated that the average potential for intercalation can be obtained from the energy change in the reaction:

$$Li + M_xM'_{1-x}O_2 \rightarrow LiM_xM'_{1-x}O_2 \quad (1)$$

First-principles computation is able to calculate the energy of the three compounds in Eq. (1), and hence the average potential, for any metal M or combination of them, in any structure, whether these conditions have been experimentally realized or not.

* Corresponding author. Tel.: +33-321-791782; fax: +33-321-791782.
E-mail address: amrioutayeb@yahoo.com (T. Amriou).

0378-7753/$ – see front matter © 2004 Elsevier B.V. All rights reserved.
doi:10.1016/j.jpowsour.2003.11.063

In this paper, the Al effect on the structure and electrochemical properties of $LiNiO_2$ compound has been investigated. Numerical calculations were performed on the $LiNiO_2$, $LiAlO_2$ and extended to quaternary spinel phase $LiAl_{0.5}Ni_{0.5}O_2$.

2. Computational details

Our calculations were performed using density-functional theory (DFT) [28–30] with the exchange-correlation functional treated in the local-density approximation (LDA) as parametrized by Hedin and Lundqvist [31,32]. The eigenvalue problem was solved applying the full-potential linearized augmented-plane-wave (FP-LAPW) method as implemented in the WIEN2K code [33–35]. This method has been known to be one of the most accurate quantum mechanical methods since it improves upon linearization and makes possible a consistent treatment of semicore and valence in one energy windows and allows inclusion of local orbits in basis. In order to achieve a satisfactory degree of convergence, the cutoff parameters used in the LAPW calculation are summarized shortly in the following: in the muffin tin spheres the wave functions were expanded in spherical harmonics with an angular momentum up to $l_{\max}^{\mathrm{wf}} = 10$. Non-spherical contributions to the electron density and potential within the MTs were considered up to $l_{\max}^{\mathrm{pot}} = 4$. The cutoff for the Fourier-series expansion of the interstitial electron density and potential was chosen to be $G_{\max} = 14\,\mathrm{bohr}^{-1}$ and the cutoff for the plane wave basis set $RK_{\max} = 8$. In general, the local-density approximation presents some deficiencies as a modest increase in computational workload.

To calculate the electronic structure of the quaternary spinel phase, a layered trigonal supercell was used which contains one nickel and aluminium ions, two lithium and four oxygen ions, thereby providing the $LiAl_{0.5}Ni_{0.5}O_2$ content. In such compound, only three points are used to represent the Brillouin zone comparatively to ten points for $LiNiO_2$ and $LiAlO_2$.

To determine the average intercalation voltage (AIV), the total energy of three structures is required using the FP-LAPW method: metallic lithium in body centered cubic and the oxide structures before and after intercalation. The energies of these oxides are calculated in the α-$NaFeO_2$ structure. The symmetry of this structure is $R\bar{3}m$. Three degrees of freedom exist: the *a*- and *c*-lattice parameters and the internal coordinate *z*. Lattice constants and internal coordinate are relaxed to find the lowest energy. Combining the basic thermodynamics [36–38] and these total energies, the AIV of these compounds can be predicted.

For the electronic configuration, the states treated as bands were: Li(2s), Ni (4s, 3p, 3d), Al (3s, 3p) and O (2s, 2p). The muffin-tin radii chosen are 1.8, 1.9, 1.9 and 1.55 a.u. for Li, Ni, Al and O, respectively.

3. Result and discussions

3.1. Structural properties

Using the first-principles all electron full potential LAPW method, the geometry optimizations were performed on the layered trigonal $LiNiO_2$, $LiAlO_2$ and $LiNi_{0.5}Al_{0.5}O_2$ as well as the corresponding host structure. The results for the *a* and *c* lattice constants, the oxygen positional parameter *z* and the volume are listed in Table 1. Where available, experimental data is added in parenthesis.

For $LiNiO_2$, the *a* and *c* lattice constants are approximately 2% smaller than NiO_2. In the case of the $LiAlO_2$, the *a* and *c* lattice constants are respectively 1 and 6% greater than the delithiated structure. The effect of the aluminum doping on the lithium nickel oxide has been investigated by substituting 50% of the nickel by aluminium atoms. The *a*-parameter is slightly increased by about 1% and an important increase (15%) of the *c*-parameter is observed when lithium is intercalated into the host structure. As is typical in LDA, the optimized volumes from our calculations are smaller than the experimental values.

The *a* lattice constant, in all intercalated compounds, is slightly modified by the lithium intercalation and this variation can be directly related to the metal–metal distance. In the Table 2, the metal to metal distance and lithium–oxygen bond lengths for the intercalated and deintercalated compounds as well as the metal–oxygen bond lengths are given. The hexagonal layered structure can be described by a slab formed by a plane of transition metal atoms, in

Table 1
Computed crystallographic (the lattice constants *a* and *c*, and the oxygen positional parameter *z*) parameters for Li_xNiO_2, Li_xAlO_2, and $Li_xNi_{0.5}Al_{0.5}O_2$ compounds in the α-$NaFeO_2$ structure (with $x = 0$ and 1)

Compounds	*a* (Å)	*c* (Å)	*z*	*V* (Å^3)
$\square NiO_2$	2.79, 2.87 (2.84)	13.13, 11.70 (13.47)	0.263, 0.255	29.61, 27.82 (31.38)
$LiNiO_2$	2.82, 2.93 (2.88)	14.06, 13.20 (14.19)	0.259, 0.260 (0.259)	32.30, 32.71 (33.97)
$\square AlO_2$	2.85 (2.87)	11.33 (11.70)	0.253 (0.255)	26.69 (27.82)
$LiAlO_2$	2.78 (2.8)	13.32 (14.23)	0.258	29.70 (32.21)
$\square Ni_{0.5}Al_{0.5}O_2$	2.98	12.58	0.257	32.28
$LiNi_{0.5}Al_{0.5}O_2$	3.01 (2.855)	14.84 (14.24)	0.254	38.95 (33.62)

The $\square$ indicates the host structure without intercalation. The $\square$ correspond to $x = 0$.

Table 2
Computed average intercalation voltage, in volts, for $LiMO_2$ compounds, and metal–oxygen, sodium–oxygen and metal–metal distances in (□/Li)MO_2 compounds, all entries in (Å)

	$LiNiO_2$	$LiAlO_2$	$LiNi_{0.5}Al_{0.5}O_2$
AIV's	3.32 (3.9 [11])	5.3 (5.4 [24])	4.0
d(M–O) (□/Li)	1.85/1.93	1.88/1.89	1.62/1.68
d(Li–O) (□/Li)	–/2.08	–/2.01	–/1.70
d(M–M) (□/Li)	2.79/2.82	2.85/2.78	2.98/3.01

The □ indicates the host structure without intercalation. The □ correspond to $x = 0$.

between two planes of oxygen. Interaction between atoms in a slab (M–O) are mainly covalent, while the slab-to-slab interactions (Li–O) are generally weaker. The M–O distance (shorter than the Li–O distance) decreases from Ni to $Ni_{0.5}Al_{0.5}$. The covalent character appears to be more important in the $Ni_{0.5}Al_{0.5}$ in comparison to the Al and Ni compounds. This theoretical result confirms the important role of the aluminium effect in order to stabilize the lithium nickel oxide in the α-$NaFeO_2$ structure and corroborates experimental observations [2–5].

When Li is intercalated, the M–O bond length increases in Ni and $Ni_{0.5}Al_{0.5}$ compounds. This structural effect is due to the lithium influence into the space between the O–M–O slabs, which pulls the oxygen towards it and leading an increase of the M–O distance. For Al compound, same M–O bond length is reported. This feature is attributed to the small nuclear Al charge which induces an effectively smaller metal ion.

Table 2 gives the predicted average intercalation voltage for Ni, Al and $Ni_{0.5}Al_{0.5}$ compounds. For lithium insertion in spinel structures, it can be seen that there is a reasonable agreement between experimental and calculated values, with the experimentally potential consistently being underestimated by about by about 1/2 V for $LiNiO_2$ compound. For $LiAlO_2$, the AIV is in the same order with the theoretical value reported by Aydinol et al. [38]. Moreover, the Al compound induces clearly an AIV which is higher than that of any lithium transition-metal oxide. From the value of the average intercalation voltage obtained for the mixed compound ($LiNi_{0.5}$ $Al_{0.5}O_2$), it is clearly that the potential increases systematically with the substitution of the nickel by the aluminium. This variation confirmed the positive effect of aluminium as it is demonstrated experimentally [2–5] and predicted theoretically [6–10]. In this case, the AIV increases by about 0.7 V in comparison to pur nickel compound.

3.2. Electronic properties

3.2.1. Band structure

In Fig. 1a and b, the LDA calculations of the band structures of $LiNiO_2$ and $LiAlO_2$ as well as the delithiated corresponding compounds in the α-$NaFeO_2$ structure are shown. The band structures and band ordering are very similar in the first region characterized by an energetically low lying bands below the Fermi level. These bands, derived from the 2s states of the oxygen atoms, do not contribute to the bonding. For the aluminium compounds, the second region is composed of six bands mainly due to 2p-O. In the case of the nickel compounds, nine bands are obtained and they are originated mainly from 2p-O in some part of the Brillouin zone and 3d-Ni in another part of the zone, as can be seen by an overlap and a mixing between these bands in the Γ-point (six bands are the 2p-O character and three bands are the d(t_{2g})-Ni character). The band ordering is really different at the Γ-point in NiO_2 comparatively to $LiNiO_2$. In NiO_2, the first three bands are originated from 2p-O with an important contribution of the d(e_g)-Ni which implies the presence of strong σ bond without excluding the π bond. The second three bands are dominated by the d(t_{2g})-Ni bands and the last are derived from 2p states of the oxygen. For $LiNiO_2$, the first part remains the same with an increasing of the partial charges d(e_g)-Ni and a decreasing of d(t_{2g})-Ni which indicates the presence of very strong σ and reduced π bonds. These bands are followed by p–O bands. In the third order, the d(t_{2g})-Ni bands are obtained. The highest band shown in Fig. 1a, are originated from d(e_g)-Ni in the NiO_2 and $LiNiO_2$ compounds. From Fig. 1b, the highest band above Fermi level is originated from s-Al, because in AlO_2 and $LiAlO_2$, the repulsive interaction with the O s-bands shifts this band to higher energies above the E_F. This band is followed by p-Al band which does not contribute to the bonding.

Comparing the band structure of the intercalated and deintercalated compounds, all the bands are shifted to higher energies due to the lithium intercalation. The Fermi energy increases with the increasing of the number of valence electron from deintercalated to intercalated compound. Finally, the intercalated compound is more covalent due to the increasing of the σ bond comparatively to the parent compound.

The electronic structure of the quaternary alloy and the corresponding host structure is similar to those obtained for the oxide compounds. The narrow band which has little interaction with other states is dominated by the s-O character. The next bands consist of 2p-O and lower 3d($t_{2}g$)-Ni orbitals. In these bands, the Ni-O mixing is also shown. The band at the Fermi level is mainly 3d(e_g)-Ni character following by the s-Al and p-Al, respectively. As Li is intercalated into the host, the Fermi level moves up in energy (3.54–4.80 eV) and the all bands are shifted up. Moreover, the band ordering is similar comparatively to the host structure.

3.2.2. The density of states

The total DOS are shown in Fig. 2 for $Li_yNi_xAl_{1-x}O_2$, where $x = 0; 1$ and $y = 0; 1$. The lithium intercalation effect can be examined into nickel compound by comparing the total and partial DOS for $LiNiO_2$ and NiO_2 shown in Fig. 2a. It is clear that the O-2s band dominates the first region in the lithiated and delithiated compound. In the second region for the $LiNiO_2$, the O-2p band extends over the wide energy

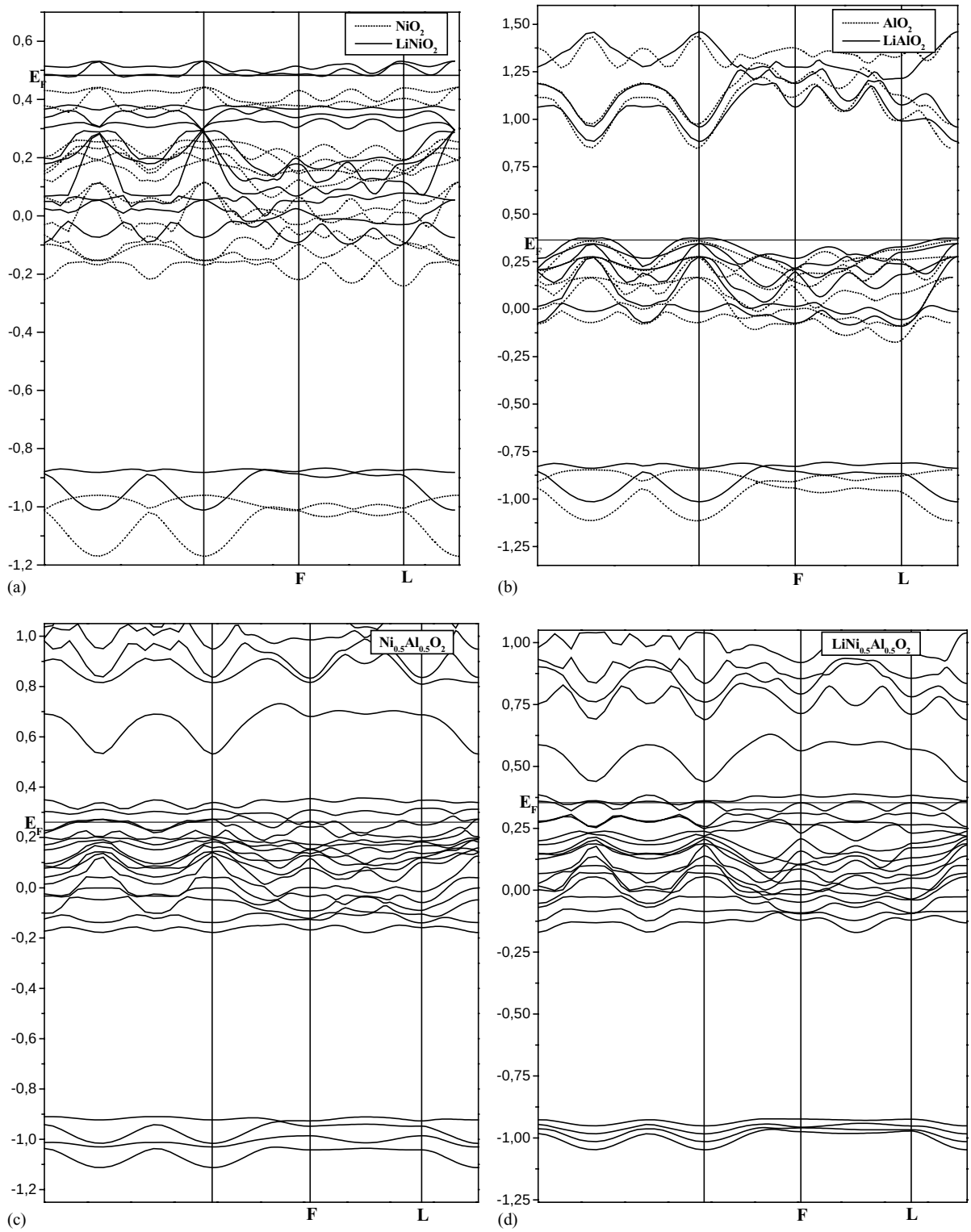

Fig. 1. The LDA energy band structure of $LiNi_xAl_{1-x}O_2$ compounds in the layered structure, where $x = 0$, 1 and 0.5.

range with a important contribution of the Ni-3d(e_g) bands. Moreover, the Ni-3d band is mainly located in the higher energy region. The lithium intercalation into NiO_2 makes the O-2p band to shift up largely (from -0.24 to -0.10 Ryd in NiO_2 and $LiNiO_2$, respectively). The overlap between the O-2p and Ni-3d bands in NiO_2 has reduced to a minimum of the density of states which separe these two bands in $LiNiO_2$. In addition, the Fermi level E_F shift up, from the top of the d(t_{2g}) to the bottom of the d(e_g) band in the $LiNiO_2$. This feature is attributed to the fact that the intercalated

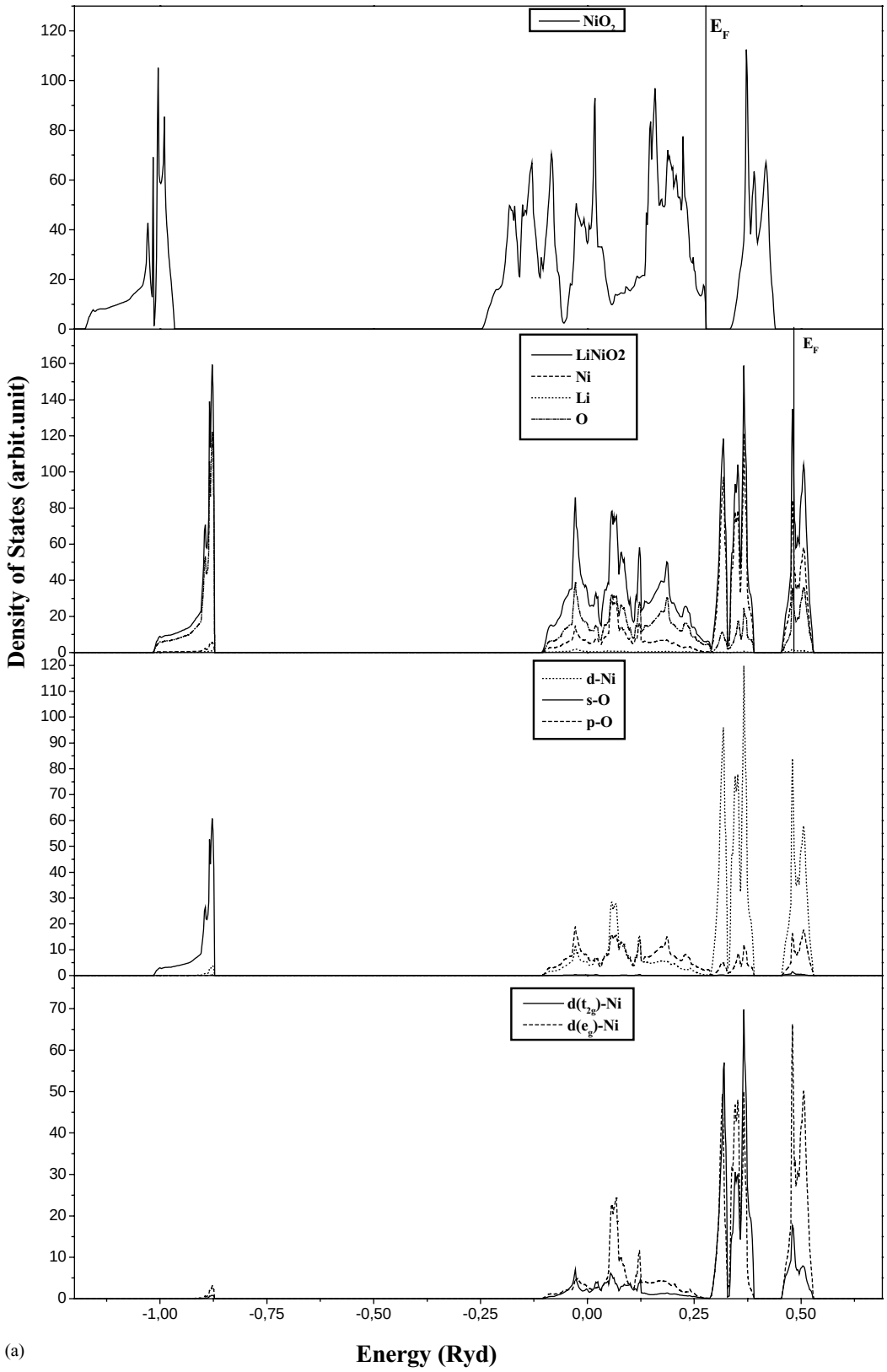

Fig. 2. Total and partial DOS for $LiNi_xAl_{1-x}O_2$ compounds in the layered structure (in states per Ryd unit cell): (a) $LiNiO_2$ and (b) $LiAlO_2$.

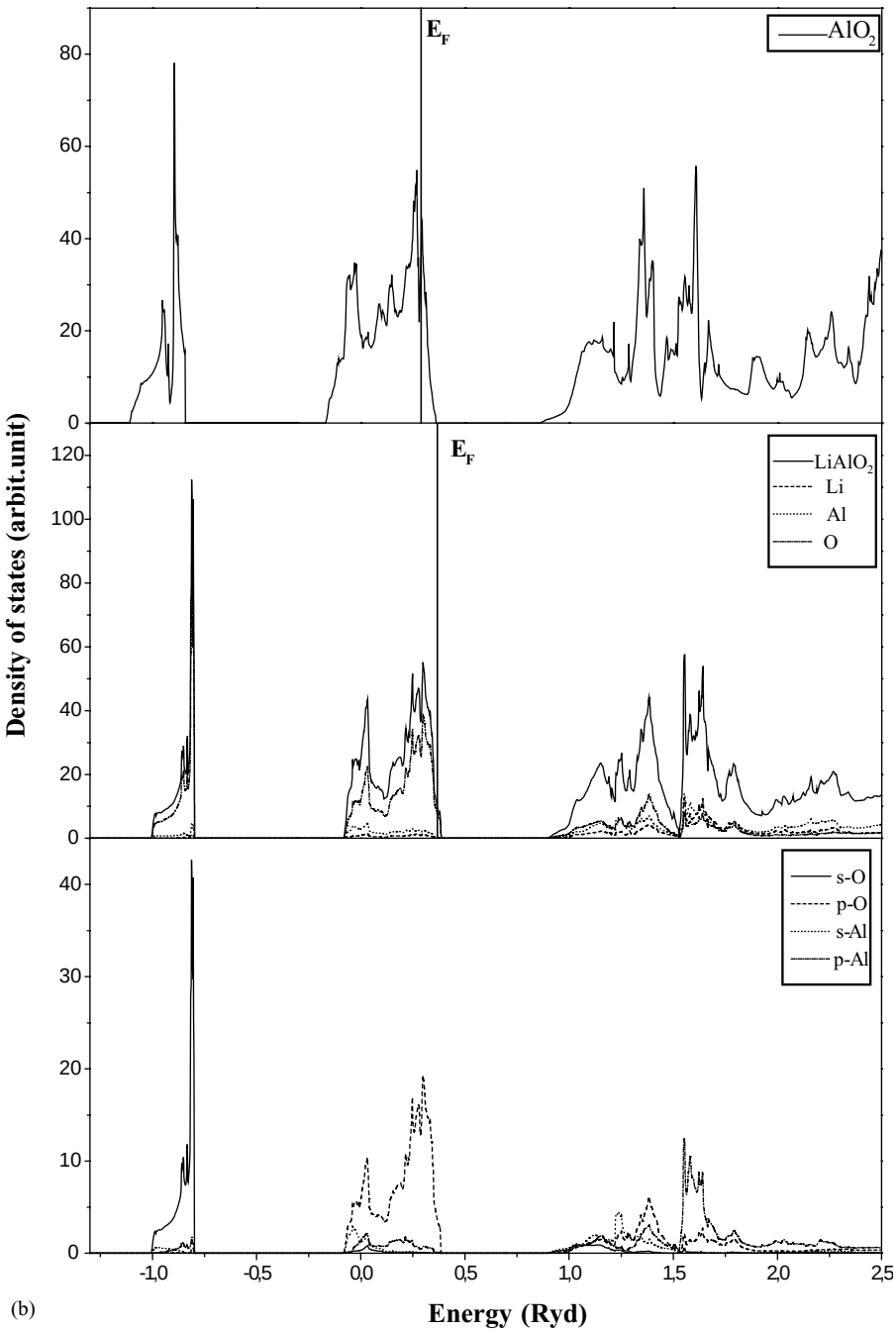

Fig. 2. (*Continued*).

electron has to be accommodated in the high energy Ni-d(e_g) band. For $LiAlO_2$ and AlO_2, (Fig. 2b), the band ordering is very similar for the first and the second region. The main difference concerns the third region which is constituted to the Al-3s and Al-3p characters.

3.2.3. Valence electron density

To study the Li intercalation effect on the valence electron density, we have calculated the difference between the valence electron density in $LiNiO_2$, $LiAlO_2$ and $LiNi_{0.5}Al_{0.5}O_2$. For this purpose, we have chosen the (1 1 0) crystallographic plane which contains lithium, oxygen and nickel (aluminium) ions for all compounds. For these calculations, all atomic positions were assumed to remain the same after lithiation.

From Fig. 3a, it seems that there is no doubt that the charge transfer is from the Li to the Ni and O ions in $LiNiO_2$ and only to O ions in $LiAlO_2$. For the quaternary alloy ($LiNi_{0.5}Al_{0.5}O_2$), the same feature is observed. From Table 3, the difference in the electronic charge inside the

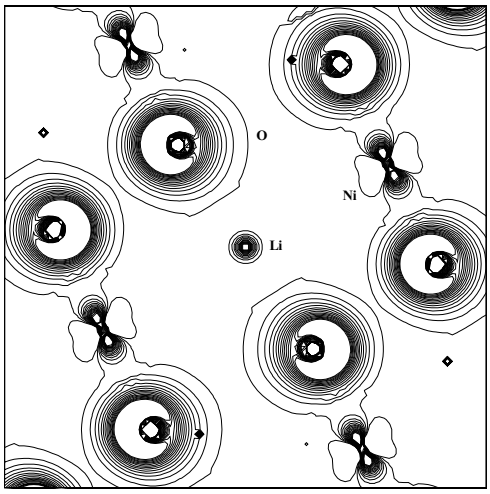

(a)

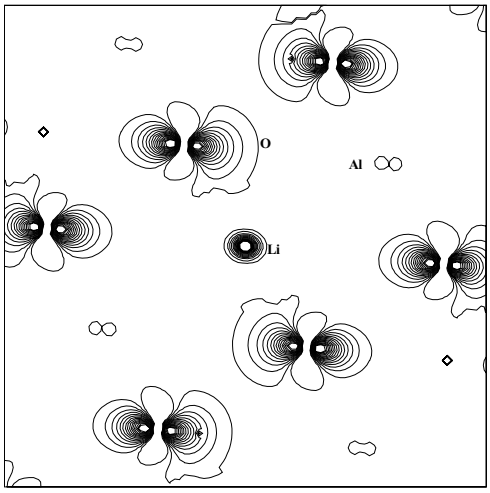

(b)

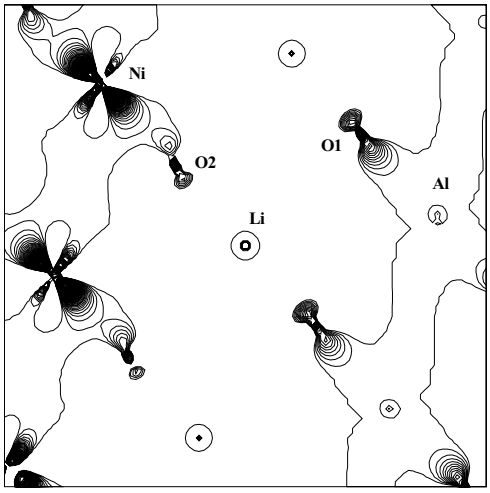

(c)

Fig. 3. Difference in the charge density between the lithiated and the unlithiated materials. The plane shown is parallel to the *c*-axis and contains lithium, oxygen and nickel (aliminium) ions. (a) $LiNiO_2/NiO_2$, (b) $LiAlO_2/AlO_2$, and (c) $LiNi_{0.5}Al_{0.5}O_2/Ni_{0.5}Al_{0.5}O_2$.

Table 3
Electron charge-transfer values to oxygen (O) and transition metals (M) upon intercalation of Li into MO_2 compounds in the α-$NaFeO_2$ structure

	Ni–O	Al–O	$(Ni_{0.5}Al_{0.5})$–O	
M	0.21	–	0.31 (Ni)	– (Al)
O	0.21	0.36	0.154 (O1)	0.227 (O2)

Note that there are two anions per unit cell.

atomic sphere between the crystal (LAPW) value $Q^{\text{sphere}}_{\text{crystal}}$ in $LiNi_xAl_{1-x}O_2$ and the superposed atomic value $Q^{\text{sphere}}_{\text{super}}$ in $Ni_xAl_{1-x}O_2$ (where $x = 0$, 1 and 0.5), which is the quantity defined the charge transfer in a compounds before and after the intercalation is presented. From these values, a charge transfer of about 0.2 an electron from the lithium to the nickel and the oxygen atoms occurs in the Nickel compound. This result is similar to those obtained by Aydinol et al. [37,38]. In the case of the aluminium, there is exclusively a charge transfer to the oxygen atoms of about 0.36 electron. For the quaternary alloy, the increasing of the charge transfer to the nickel by about 32.5% is observed comparatively to $LiNiO_2$. Moreover, the charge transfer to oxygen is slightly increased in comparison to pur compound ($LiNiO_2$ and $LiAlO_2$).

4. Conclusion

In this paper, we showed that the linearized augmented plane waves method can be used to estimate the average insertion potentials as well as the electronic structure of NiO_2, AlO_2 and $Ni_{0.5}Al_{0.5}O_2$ cathodes for secondary lithium batteries. The agreement between the experimentally mesured and the calculated average potential is consistently underestimated by about 1/2 V for $LiNiO_2$, whith confirms the accurate prediction of the LAPW method for all compounds. Moreover, we find that the substitution of Ni by Al lead to higher Li intercalation voltage comparativelly to the pur compound ($LiNiO_2$) and stabilize the structure. We have shown that the charge transfer from Li to Ni atoms has an effect on the AIV without exclude the great importance of the charge transfer from Li to O atoms as demonstrated by many authors.

Acknowledgements

The authors would like to thank Prof. P. Blaha and all the Wien group members for providing us with their LAPW package. This work is partially supported by the CMEP (France).

References

[1] Proceedings of the 9th IMLB, Edinburgh, Scotland, 12–17 July 1998, J. Power Sources 81/82 (1998).
[2] R. Koksbang, J. Barker, H. Shi, M.Y. Saïdi, Solid State Ionics 84 (1) (1996) 1–21.

[3] S.G. Youn, I.H. Lee, C.S. Yoon, C.K. Kim, Y.-K. Sun, Y.-S. Lee, M. Yoshio, J. Power Sources 108 (2002) 97–105.
[4] S. Castro-Garcia, A. Castro-Couceiro, M.A. Senaris-Robriguez, F. Soulette, C. Julien, Solid State Ionics 156 (2003) 15–26.
[5] W.Y. Liang, in: M. Balkanski (Ed.), Microionics-Solids State Integrable Batteries, North-Holland, Amsterdam, 1991, pp. 237–251.
[6] C. Julien, M. Balkanski, in: G.A. Nazri, J.M. Tarascon, M. Armand (Eds.), Solid State Ionics III Symposia Proceedings, vol. 293, Materials Research Society, Pitsburgh, PA, 1993, pp. 27–37.
[7] D.J. Sellmeyer, in: H. Ehrenreich, F. Seitz, D. Turnbull (Eds.), Solid State Physics: Advances in Research and Apllications, vol. 3, Academic Press, New York, 1978, p. 83.
[8] J.V. Mc Canny, J. Phys. C 12 (1979) 3263.
[9] C. Umrigar, D.E. Ellis, D.S. Wang, H. Krahauer, M. Posternak, Phys. Rev. B 26 (1982) 4935.
[10] G.Y. Guo, W.Y. Liang, J. Phys. C 20 (1987) 4315.
[11] C. Delmas, J.P. Rougier, A. Demourgues, F. Weill, A. Chadwick, M. Broussely, F. Perton, Ph. Biensan, P. Willmann, J. Power Sources 68 (1997) 120.
[12] A. Rougier, P. Gravereau, C. Delmas, J. Electrochem. Soc. 143 (1996) 1168.
[13] H. Arai, S. Okada, Y. Sakurai, J. Yamaki, Solid State Ionics 95 (1997) 275.
[14] H. Arai, S. Okada, Y. Sakurai, J. Yamaki, J. Electrochem. Soc. 144 (1997) 3117.
[15] E. Rossen, C.D.W. Jones, J.R. Dahn, Solid State Ionics 57 (1992) 311.
[16] C.C. Chang, J.Y. Kim, P.N. Kumta, J. Electrochem. Soc. 147 (2000) 1722.
[17] C. Delmas, I. Saadoune, Solid State Ionics 53–56 (1992) 370.
[18] Y.M. Choi, S.I. Pyun, S.I. Moon, Solid State Ionics 89 (1996) 43.
[19] T. Ohzuku, A. Ueda, M. Kouguchi, J. Electrochem. Soc., 142, 4033 (1995).
[20] A. Yu, G.V. Subba Rao, B.V.R. Chowdari, Solid State Ionics 135 (2000) 131.
[21] T. Ohzuku, A. Ueda, M. Kouguchi, J. Electrochem. Soc. 142 (1995) 4033.
[22] Q. Zhong, U. Von Sacken, J. Power Sources 54 (1995) 221.
[23] G.A. Nasri, A. Rougier, K.F. Kia, Mater. Res. Soc. Sym. Proc. 453 (1997) 635.
[24] G. Ceder, Y.-M. Chiang, D.R. Sadoway, M.K. Aydinol, Y.-I. Jang, B. Huang, Nature 396 (1998) 694.
[25] H.A. Lehmann, H. Hesselbarth, Z. Anorg. Allg. Chem. 313 (1961) 117.
[26] Y.-I. Jang, B. Huang, Y.-M. Chiang, D.R. Sadoway, Electrochem. Solid State Lett. 1 (1998) 13.
[27] G. Ceder, M.K. Aydinol, A.F. Kohan, Comput. Mater. Sci. 8 (1997) 161.
[28] N.H. March, S. Lundqvist (Eds.), Theory of the Inhomogeneous Electron Gas, Plenum Press, New York, 1983.
[29] W. Kohn, L.J. Sham, Phys. Rev. A 140 (1965) 1133.
[30] R.M. Dreizler, E.K.U. Gross, Density Functional Theory, Springer-Verlag, Berlin, 1990;
R.G. Parr, W. Yung, Density of Atoms and Molecules, Oxford, New York, 1989.
[31] L. Hedin, B.I. Lundqvist, J. Phys. C4 (1971) 2064–2083.
[32] C. Bowen, G. Sugiyama, B.J. Alder, Phys. Rev. B 50 (1994) 14838; S. Soroni, D.M. Ceperley, G. SeNatore, Phys. Rev. Lett. 75 (1995) 689.
[33] D.J. Singh, Plane waves, pseudopotentials and the LAPW method, Kluwer Academic, Publishers, Boston, Dordrecht, London, 1994.
[34] E. Wimmer, H. Krakauer, M. Weinert, A.J. Freeman, Phys. Rev. B 24 (1981) 864;
M. Weinert, E. Wimmer, A.J. Freeman, Phys. Rev. B 26 (1982) 4571.
[35] P. Blaha, K. Schwarz, P. Sorantin, Comput. Phys. Commun. 59 (1990) 399.
[36] E. Deiss, A. Wokaun, J.L. Barras, C. Daul, P. Dufec, J. Electrochem. Soc. 144 (1997) 3877.
[37] M.K. Aydinol, G. Ceder, J. Electrochem. Soc. 144 (1997) 3832.
[38] M.K. Aydinol, A.F. Kohan, G. Ceder, K. Cho, J. Joannopoulos, Phys. Rev. B 56 (1997) 1345.